

Probing the Two-Temperature Paradigm: Observational Tests for the Basic Assumptions in ADAFs.

Rohan Mahadevan

Institute of Astronomy, University of Cambridge,
Madingley Road, Cambridge, CB3 0HA, UK.
rohan@ast.cam.ac.uk

ABSTRACT

We calculate the flux and spectrum of synchrotron radiation produced by high energy electrons and positrons (e^\pm) in an advection dominated accretion flow (ADAF) around a black hole. The e^\pm are from the decay of charged pions which are created through proton–proton collisions. We consider both a thermal and power–law energy distribution of protons, and show that the resulting e^\pm synchrotron emission produces a characteristic spectrum between radio and X–ray frequencies. While previous signatures of the hot protons were only possible at gamma–ray energies, via the production of gamma–rays through neutral pion decay, the present results provide a more observationally tractable way of probing the proton energy distribution and the two temperature structure in these accretion flows. We discuss a number of strong observational predictions from these systems, as well as the recent results of Mahadevan (1998) which appear to confirm the two temperature structure in ADAFs. We show that the results provide support for both a power–law and thermal distribution of protons, with at least a third of the viscous energy going into the power–law.

Key words: accretion, accretion discs – elementary particles – radiation mechanisms: nonthermal – acceleration of particles – Galaxy: centre – radio continuum: galaxies

1. Introduction

In an advection–dominated accretion flow (ADAF), all the viscous energy generated is stored in the accreting gas and advected into the central star (Ichimaru 1977; Rees et al. 1982; Abramowicz et al. 1998; Narayan & Yi 1994, 1995ab; Abramowicz et al. 1995; see Narayan, Mahadevan & Quataert 1998a for a recent review). If the central object happens to be a black hole, the advected energy is lost through the event horizon, and the accreting system appears very dim. Most of the viscous heating is assumed to mainly affect the ions, the more massive species, while the radiation is produced primarily by the electrons. Since the ions transfer only small fraction of their energy to the electrons

via Coulomb collisions, the radiative efficiency of an ADAF is much less than the total energy released during accretion (Rees et al. 1982). The gas in an ADAF forms a two temperature structure (Shapiro, Lightman, & Eardley 1976; Rees et al. 1982), with the ions attaining nearly virial temperatures close to the black hole ($T_i \sim 10^{12}$ K), and the electrons being much cooler ($T_e \sim 10^{9.5}$ K).

The success of ADAF models lies in their ability to accurately predict the observed spectrum from a number of accreting stellar mass and supermassive black hole systems (see Narayan et al. 1998a for a review). The spectrum depends sensitively on the assumed energy distribution of the protons and electrons as well as their individual cooling mechanisms. The protons cool by creating neutral pions, which subsequently decay into gamma-rays (Mahadevan, Narayan, & Krolik 1997), while the electrons cool by various optically thin processes such as cyclo-synchrotron, inverse Compton and bremsstrahlung radiation (see eg. Narayan & Yi 1995b; Mahadevan 1997). The electrons form a thermal distribution (Mahadevan & Quataert 1998), and give rise to a spectrum ranging from radio to hard X-ray frequencies (10^9 Hz $\lesssim \nu \lesssim 10^{21}$ Hz), but the energy distribution of the protons, and therefore the resulting gamma-ray spectrum, is still unknown and depends on the viscous heating mechanism involved (Mahadevan & Quataert 1997; Mahadevan et al. 1997). If viscosity heats the protons into a thermal distribution, the resulting gamma-ray spectrum is sharply peaked around energies ~ 70 MeV, while a power-law distribution results in a power-law gamma-ray spectrum which extends to very high energies (Mahadevan et al. 1997).

It is the purpose of this paper to probe the two temperature paradigm further and attempt to resolve what the distribution function of the protons is likely to be. We are therefore interested in other possible emission processes from the protons from which accurate spectra can be determined. In particular, we focus on the production of charged pions which subsequently decay into electrons and positrons. These particles interact with the equipartition magnetic fields in the accreting gas, and produce synchrotron radiation. Although this energy leaves the plasma at lower frequencies than gamma-rays, it provides the exciting possibility that current sensitive and high resolution radio to X-ray telescopes might be used to probe the much higher energy proton distribution function and viscous heating mechanisms in these plasmas.

We begin in §2 by describing all the physical processes involved in calculating the e^\pm synchrotron spectra from both a thermal and power-law parent proton distribution. These calculations depend only on the microphysics of particle collisions, decays, and emission processes. §3 introduces the physical properties of an ADAF and, using the results of §2, determines the general properties of the resulting e^\pm spectrum from an ADAF. §4 applies these results to solar mass and supermassive accreting black holes. In §5 we conclude by discussing the implications of these results on the basic assumptions in ADAFs, and propose future observational tests which would lead to a better understanding of these systems.

2. Physical Processes

2.1. Production of Electrons and Positrons

The production of electrons and positrons through the decay of charged pions is a three step process and has been studied by various authors (see eg. Ginzburg & Syrovatskii 1964; Ramaty & Lingenfelter 1966ab, 1968; Stecker 1971; Bhadwar et al. 1977; Dermer 1986ab). The colliding protons produce a charged pion, π^\pm , which decays into a charged muon, μ^\pm , and a muon neutrino, ν_μ . The charged muon decays into an electron, neutrino and their antiparticles. The reactions are

$$\begin{aligned} p + p &\rightarrow \pi^\pm + X, \quad \pi^\pm \rightarrow \mu^\pm + \nu_\mu(\bar{\nu}_\mu), \\ \mu^\pm &\rightarrow e^\pm + \nu_e(\bar{\nu}_e) + \bar{\nu}_\mu(\nu_\mu), \end{aligned} \quad (1)$$

where X represents all other decay products. The number of charged pions created per unit volume, per unit time, with energy E_{π^\pm} , is given by (Landau & Lifshitz 1975, §12; cf. Mahadevan et al. 1997, eq.[4])

$$\begin{aligned} R(E_{\pi^\pm}) \equiv \frac{dN_{\pi^\pm}}{dE_{\pi^\pm} dV} &= \frac{c}{2} \int_1^\gamma d\gamma_1 \int_\gamma^\infty d\gamma_2 \int_{-1}^1 d\cos\theta \frac{d\sigma(E_{\pi^\pm}; \gamma_1, \gamma_2, \cos\theta)}{dE_{\pi^\pm}} \\ &\times n_{\gamma_1} n_{\gamma_2} \sqrt{(\vec{\beta}_1 - \vec{\beta}_2)^2 - (\vec{\beta}_1 \times \vec{\beta}_2)^2} \text{ s}^{-1}, \end{aligned} \quad (2)$$

where $(\vec{\beta}_1, \vec{\beta}_2)$, (γ_1, γ_2) , $(n_{\gamma_1}, n_{\gamma_2})$ are the velocity parameters, Lorentz factors, and densities of the two colliding particles respectively, $\cos\theta = \vec{\beta}_1 \cdot \vec{\beta}_2 / |\vec{\beta}_1| |\vec{\beta}_2|$, $d\sigma(E_{\pi^\pm}; \gamma_1, \gamma_2, \cos\theta) / dE_{\pi^\pm}$ is the normalized differential cross section for the production of a charged pion with energy E_{π^\pm} , and c is the velocity of light. Following Mahadevan et al. (1997), the differential cross section is determined by using the isobar model for energies $\lesssim 4$ GeV (Lindenbaum & Sternheimer 1957; Stecker 1971; Dermer 1986a), and the scaling model for energies $\gtrsim 8$ GeV (Bhadwar et al. 1977; Stephens & Bhadwar 1981; Dermer 1986b). At intermediate energies the differential cross section is determined by interpolating smoothly (cubic interpolation) between the two regimes.

The spectrum of electrons and positrons, $R(e^\pm)$, is derived from the π^\pm spectrum by considering the reactions,

$$\pi^\pm \rightarrow \mu^\pm + \nu_\mu(\bar{\nu}_\mu), \quad \mu^\pm \rightarrow e^\pm + \nu_e(\bar{\nu}_e) + \bar{\nu}_\mu(\nu_\mu).$$

Ideally, determining the energy distribution of e^\pm in the laboratory frame requires three Lorentz transformations: one to rest frame of the π^\pm , to determine the decay spectrum of the μ^\pm , the second to the rest frame of the μ^\pm , to determine the decay spectrum of the e^\pm , and the third a transformation back to the laboratory frame. However, since the Lorentz factor of the μ^\pm is small in the rest frame of the π^\pm ,

$$\gamma_{\mu^\pm} = \frac{m_{\pi^\pm}^2 + m_{\mu^\pm}^2}{2m_{\pi^\pm}m_{\mu^\pm}} \simeq 1.046, \quad (3)$$

the difference between its velocity and that of the parent π^\pm can be neglected. In this approximation, $R(E_{\pi^\pm}) \simeq R(E_{\mu^\pm})$, and determining the e^\pm spectrum simplifies to requiring only two Lorentz transformations. $R(E_{e^\pm})$ can now be obtained by performing the double integral (Ginzburg & Syrovatskii 1964),

$$R(E_{e^\pm}) = \int \int \frac{1}{2\gamma_{\pi^\pm}\beta_{\pi^\pm} p'_{e^\pm}} R(E_{\pi^\pm}) \frac{dP'}{dE'_{e^\pm}} dE_{\pi^\pm} dE'_{e^\pm}, \quad (4)$$

where the limits of integration are such that

$$|E_{e^\pm} - E'_{e^\pm}| \leq p'_{e^\pm} \gamma_{\pi^\pm} \beta_{\pi^\pm}.$$

Here, dP'/dE'_{e^\pm} is the probability of creating an e^\pm with energy E'_{e^\pm} and momentum p'_{e^\pm} in the rest frame of the decaying muon, and is given by (Ginzburg & Syrovatskii 1964),

$$\frac{dP'}{dE'_{e^\pm}} = \frac{16E'_{e^\pm}}{m_\mu^3} p'_{e^\pm} \left[3 - 4 \frac{E'_{e^\pm}}{m_\mu} \right]. \quad (5)$$

2.2. Synchrotron Emission

If the plasma in which the e^\pm 's are created has a magnetic field, the particles interact with the magnetic field and cool by radiating synchrotron emission. The synchrotron radiation produces a characteristic spectrum which depends directly on the energy distribution of the e^\pm . Since the distribution of e^\pm is determined by the proton energy distribution (cf. eqs. [2], [4]), the resulting synchrotron spectrum provides a probe to the energy distribution of the protons. Here, we provide the basic equations that determine the e^\pm synchrotron spectra, and show (§2.3) how different initial proton distributions give rise to different spectra. In what follows all quantities refer to the created e^\pm , unless otherwise noted.

Calculating the synchrotron emissivity, $L_\nu^s(\nu)$, requires evaluating

$$L_\nu^s d\nu = \int_{\gamma_{\min}}^{\gamma_{\max}} N(\gamma) j(\nu, \gamma) d\gamma \quad \text{erg s}^{-1} \text{ cm}^{-3} \text{ Hz}^{-1}, \quad (6)$$

where γ is the Lorentz factor of the created e^\pm , $j(\nu, \gamma)$ is the synchrotron emission formula averaged over all particle directions, and $N(\gamma)$ is the steady state distribution of e^\pm . Since the e^\pm created are highly relativistic (§2.3, Fig. 1), and extend to very high energies, we can set $\gamma_{\min} \gg 1$, and $\gamma_{\max} \rightarrow \infty$. In this limit, $j(\nu, \gamma)$ takes the relativistic form (eg. Rybicki & Lightman 1979),

$$j(\nu, \gamma) = S_0 F\left(\frac{\nu}{\nu_c}\right),$$

$$S_0 = \frac{4\pi\sqrt{3}e^2\nu_B}{3c}, \quad \nu_c = \frac{3}{2}\gamma^2\nu_B, \quad \nu_B = \frac{eB}{2\pi m_e c}, \quad (7)$$

where we have averaged over all particle directions. Here $F(x)$ is an integral over modified Bessel functions (Rybicki & Lightman 1979, eq.[6.31c]), $S_0 = 1.56 \times 10^{-22} B$, and $\nu_B = 2.8 \times 10^6$ Hz is the cyclotron frequency. Integrating equation (7) over all frequencies gives the total energy radiated per particle,

$$\dot{E}_S \equiv \int_0^\infty j(\nu, \gamma) d\nu = 1.06 \times 10^{-15} \gamma^2 B^2 \text{ erg s}^{-1}. \quad (8)$$

For large γ , the e^\pm radiate their energy very efficiently, and their steady state distribution, $N(\gamma)$, is determined by the competing effects of the “creation” and “depletion” of particles. At a given energy E , the colliding protons produce $R(E)$ electrons and positrons. These e^\pm , however, cool very efficiently, thereby reducing the number of e^\pm at energy E . The steady state distribution can therefore be determined by solving the Fokker–Planck equation without the stochastic term,

$$\frac{\partial N(\gamma, t)}{\partial t} = -\frac{\partial}{\partial \gamma} [\dot{\gamma} N(\gamma, t)] + R(\gamma, t), \quad (9)$$

with $\partial N(\gamma, t)/\partial t = 0$. Here, $\dot{\gamma} = \dot{E}_S/m_e c^2$ is the cooling rate of the e^\pm and $R(\gamma)$ is their injection rate (cf. eq. [4]). In steady state, the equation requires the net flux of particles between γ_1 and γ_2 to be equal to the rate of injection of particles between these two Lorentz factors. Alternatively, the equation can be thought of as a particle conservation equation in energy space with $\dot{\gamma}$ being the velocity along the energy axis.

Setting $\partial N(\gamma, t)/\partial t = 0$, equation (9) gives

$$N(\gamma) = -\frac{1}{\dot{\gamma}} C(\gamma),$$

$$C(\gamma) \equiv \int_\gamma^\infty R(\gamma') d\gamma', \quad (10)$$

where $C(\gamma)$ is the total number of injected e^\pm above Lorentz factor γ . Using equation (6), the resulting synchrotron spectrum can be written as

$$L_\nu^s d\nu = \int_{\gamma_{\min}}^\infty C(\gamma) \frac{j(\nu, \gamma)}{\dot{\gamma}} d\gamma \text{ erg cm}^{-3} \text{ s}^{-1} \text{ Hz}^{-1}. \quad (11)$$

2.3. Synchrotron Spectra from Electrons and Positrons.

Using equations (2), (4), (10), and (11), the synchrotron spectra from the e^\pm can be determined, and depends only on the initial proton energy distribution. We consider here two extreme distributions: a relativistic Maxwell–Boltzmann, $N(E) \propto E^2 \exp(-E/kT)$, and a power–law with energy index s , $N(E) \propto E^{-s}$. In almost all areas of astrophysics, the true proton distribution is probably some combination of the two.

Before determining the exact synchrotron spectra, we point out two general properties of equation (11). First, the total synchrotron power, P_{total} , is given by

$$P_{\text{total}} = \int_0^{\infty} L_{\nu}^s d\nu = m_e c^2 \int_{\gamma_{\min}}^{\infty} C(\gamma) d\gamma \text{ erg s}^{-1}, \quad (12)$$

which is equal to the total energy of e^{\pm} that are created per second. This depends only on the injected energy spectrum and is independent of the synchrotron emissivity, $j(\nu, \gamma)$, and therefore of the magnetic field. We might expect that since particles in a very low magnetic field radiate synchrotron emission inefficiently (cf. eq.[8]), the total synchrotron emission from this plasma would be low. However, since we are interested in steady state distributions, the decrease in the amount of cooling is exactly compensated by an increase in the steady state number density (cf. eq. [10]). Similarly, higher magnetic fields lead to more efficient cooling, which results in a lower steady state number density of particles. The two effects exactly compensate for each other and leaves the total cooling rate unchanged.

Second, the synchrotron spectrum, in a νL_{ν} versus ν plot, is only a function of the dimensionless frequency $\chi \equiv \nu/\nu_B$ (cf. eqs. [7, 11]). This shows that while the intrinsic shape of the synchrotron spectrum does not change as the magnetic field changes, the position of the spectrum does move horizontally to the right (left) as the magnetic field is increased (decreased).

2.3.1. Thermal Proton Distribution

Using a normalized relativistic Maxwell–Boltzmann distribution for $n_{\gamma_1}, n_{\gamma_2}$ in equation (2), $R(E_{\pi^{\pm}})$ is obtained by performing the integrals given in Dermer (1986a; see also Mahadevan et al. 1997, eq. [12] with the appropriate changes for π^{\pm} cross–sections). The results are then used in equation (4) to determine the resulting production spectrum, $R(E_{e^{\pm}})$, of electrons and positrons.

Figure 1a shows $R(E_{e^{\pm}})$ for different values of the dimensionless proton temperature $\theta_p = kT_p/m_p c^2 = 0.05, 0.1, 0.2$. The spectra rise at low energies, peak near $E_{e^{\pm}} \sim 33$ MeV, and then decline exponentially at higher energies.

An important feature shown in Figure 1a is the effect of small changes in temperature on $R(E_{e^{\pm}})$. At low temperatures, only protons in the exponential tail of the Maxwell–Boltzmann distribution have energies above threshold to produce pions and therefore electrons and positrons. Increasing the temperature by a factor of two from 0.05 to 0.1, dramatically increases the number of protons with energies above threshold, thereby increasing $R(E_{e^{\pm}})$ by more than an order of magnitude. Changing the temperature again, from 0.1 to 0.2, has a less drastic effect on the production rate. At these high temperatures the protons responsible for most of the π^{\pm} production are no longer in the tail of the Maxwell–Boltzmann distribution, but rather have energies of order the

average energy of the plasma. Therefore changing the temperature by a factor of two, has the effect of increasing $R(E_{e^\pm})$ by nearly the same amount.

Figure 1b shows the resulting steady state distribution of e^\pm (cf. eq.[10]). At low energies, the product $\dot{\gamma}N(\gamma)$ is a constant, which gives a power–law distribution $N(\gamma) \propto \gamma^{-2}$, while at higher energies $N(\gamma)$ decreases exponentially. The low energy power–law is the result of high energy e^\pm that lose their energy due to efficient synchrotron cooling.

Figure 1c shows the resulting e^\pm synchrotron spectrum for three values of the magnetic field $B = 10, 10^4, 10^8$ Gauss (solid, dashed, and dotted lines respectively), and for $\theta_p = 0.2$ (lower values of θ_p result in identical spectra, but with much lower fluxes). As expected, increasing the magnetic field merely shifts the spectrum to higher frequencies, and leaves the total flux and shape of the spectrum unchanged. The change in the steady state distribution $N(\gamma)$ from a power–law at low energies ($\propto \gamma^{-2}$) to an exponential at high energies, results in a synchrotron spectrum that rises as $\nu L_\nu \propto \nu^{+0.5}$, and then turns over exponentially (Rybicki & Lightman 1979). The frequency, ν_t , at which the spectrum turns over is determined by the Lorentz factor of the e^\pm responsible for most of the radiation ($\gamma \sim 100$, see Fig. 1b), as well as the magnetic field strength, and is given by $\nu_t \sim 3 \times 10^6 \gamma^2 B \sim 10^{10} B$.

2.3.2. Power–law Proton Distribution

Using a normalized power–law proton distribution, $n_\gamma = (s - 1)\gamma^{-s}$, with energy index s , equations (2) and (4) are used to determine the production rate, $R(E_{e^\pm})$, of electrons and positrons. The calculation is identical to that of π^0 production with the appropriate changes for π^\pm cross–sections (see Mahadevan et al. 1997).

Figure 1d shows $R(E_{e^\pm})$ for three values of the energy index s . The spectrum rises at low energies, turns over at $E_{e^\pm} \sim 35$ MeV, and extends as a power–law, E^{-s} , with the same energy dependence as the parent proton distribution (Ginzburg & Syrovatskii 1964). While the energy at which the spectra turn over are similar to the thermal case (cf. Fig. 1a), the non–thermal spectra are much broader and extend to very high energies. In addition, the production rate is not very sensitive to the energy index s . An increase in s results in a small decrease in the number of protons above the threshold energy, which moderately decreases the total production rate.

Figure 1e shows the resulting steady state e^\pm distribution. Similar to the thermal case, the product $\dot{\gamma}N(\gamma)$ is constant at low energies which gives a power–law distribution $N(\gamma) \propto \gamma^{-2}$. At higher energies, however, the shape of the distribution deviates substantially from the thermal case, and extends to very high energies as $N(\gamma) \propto \gamma^{-(s-1)}$ (cf. eq. [10]).

The resulting e^\pm synchrotron spectrum is shown in Figure 1f for three values of the magnetic field $B = 10, 10^4, 10^8$ Gauss, and for $s = 2.75$. As in the thermal case, increasing the magnetic field merely shifts the spectrum to higher frequencies and leaves the total flux and shape of the spectrum unchanged. The change in the index of the steady state distribution from low to high energies, results in a synchrotron spectrum that rises as $\nu L_\nu \propto \nu^{+0.5}$, which then steepens to $\nu L_\nu \propto \nu^{-s/2}$ (Rybicki & Lightman 1979). Therefore, while different values for the proton energy index s result in identical spectra at low frequencies, smaller values of s give rise to harder spectra at high frequencies. For all s , the frequency at which the spectrum turns over is given by, $\nu_t \sim 3 \times 10^6 \gamma^2 B \sim 10^{11} B$, where we have set $\gamma \sim 200$ (cf. Fig. 1d).

3. Application to ADAFs

The results from the previous section can now be used to determine the total e^\pm synchrotron spectrum from an ADAF. Since an ADAF is well approximated by a series of concentric spherical shells (Narayan & Yi 1995ab), with the properties of the gas varying with radius, the total e^\pm spectrum is obtained by determining the synchrotron spectra from each shell, and then propagating the resulting spectra through the accretion flow to the observer (§3.2). Determining the spectrum from each shell requires a knowledge of the proton densities and magnetic field strengths at each radius. These quantities are obtained by solving for the global structure of an ADAF.

3.1. ADAF Equations and Properties

The global structure of an ADAF is characterized by four parameters: the viscosity parameter α (Shakura & Sunyaev 1973), the ratio of gas to total pressure β_{adv} , the mass of the central black hole M , and the accretion rate \dot{M} . Given these parameters, the global structure of an ADAF can be calculated (Gammie & Popham 1998; Popham & Gammie 1998; Narayan, Kato, & Honma 1997; Chen, Abramowicz, & Lasota 1997), and for the results presented here, we use the new fully relativistic, self-consistent, global solutions in the Kerr metric developed by Popham & Gammie (1998). In general, ADAFs appear to have large values of $\alpha \gtrsim 0.1$, and the uncertainty in the value is a factor of a few (Narayan 1996). Most ADAF models in the literature use $\alpha = 0.3$ (see Narayan et al. 1998a). For the magnetic field strength, we consider two extreme values of $\beta_{\text{adv}} = (0.5, 0.9)$, which corresponds, respectively, to an equipartition field, and to one where the field contributes negligibly ($\sim 1/10$) to the total pressure.

Assuming that the mass fraction of hydrogen is $X = 0.75$, the total numberdensity

of protons is obtained from the continuity equation,¹ and is given by,

$$\begin{aligned} n_p(r) &= \frac{X\rho(r)}{m_p} = 1.9 \times 10^{19} m^{-1} \dot{m} r^{-2} \left[\frac{v(r)}{c} \right]^{-1} \frac{1}{\cos \theta_H} \left(\frac{1 - [v(r)/c]^2}{1 - r^{-1}} \right)^{1/2} \\ &\equiv m^{-1} \dot{m} \tilde{n}(r) \text{ cm}^{-3}, \end{aligned} \quad (13)$$

where $\rho(r)$ is the mass density and $v(r)$ is the radial velocity of the gas. Here, $m = M/M_\odot$ is the mass of the black hole in solar mass units, $\dot{m} = \dot{M}/\dot{M}_{\text{Edd}}$ is the accretion rate in Eddington units with $\dot{M}_{\text{Edd}} = 10 L_{\text{Edd}}/c^2 = 1.38 \times 10^{18} m \text{ g s}^{-1}$, and $r = R/R_s$ is the radius in Schwarzschild units where $R_s = 2GM/c^2 = 2.95 \times 10^5 m \text{ cm}$. This equation differs from that in Mahadevan et al. (1997) by the two last terms on the right. The factor $(\cos \theta_H)^{-1}$ accounts for the slight non-spherical geometry of the flow (Narayan, Barret & McClintock 1997a, Appendix A), and the term in parentheses is a general relativistic correction factor (Popham & Gammie 1998). We obtain $v(r)/c$ and $\cos \theta_H$ from the global ADAF solutions of Popham & Gammie (1998).

The magnetic field strength is determined by the parameter β_{adv} , and is defined by (Narayan & Yi 1995b),

$$\begin{aligned} \frac{B^2(r)}{24\pi} &= \left(\frac{1 - \beta_{\text{adv}}}{\beta_{\text{adv}}} \right) p_g, \\ p_g &= \beta_{\text{adv}} \rho(r) c_s^2(r) = \frac{\rho(r) k T_p}{\mu_i m_p} + \frac{\rho(r) k T_e}{\mu_e m_p}, \end{aligned} \quad (14)$$

where p_g is the gas pressure, $c_s(r)$ is the isothermal sound speed, and $\mu_i = 1.23$, $\mu_e = 1.14$ are the effective molecular weights of the ions and electrons respectively. Since $T_p \gg T_e$ we neglect the second term to obtain

$$T_p(r) = 1.34 \times 10^{13} \beta_{\text{adv}} \left[\frac{c_s(r)}{c} \right]^2 \text{ K.} \quad (15)$$

We obtain $c_s(r)/c$ from the global ADAF solutions (Popham & Gammie 1998).

Given $n_p(r)$ and $B(r)$ from equations (13), (14), and (15), the e^\pm spectrum can now be determined.

3.2. ADAF Spectra

In addition to the numberdensity of protons and magnetic field strength, the spectrum from each radius, and therefore the total e^\pm synchrotron spectrum from the ADAF,

¹The continuity equation is given by,

$$\dot{M} = 4\pi R^2 \rho(R) v(R) \cos \theta_H \left(\frac{1 - R_s/R}{1 - [v(R)/c]^2} \right)^{1/2}.$$

also depends on the energy distribution of the protons (§2.3). Since our knowledge of the viscous heating of protons is unknown, it is still uncertain as to whether the process leads to a thermal or power–law distribution in proton energies, or possibly a combination of the two. Below, we explore both distributions and calculate the e^\pm synchrotron spectrum associated with them.

At each radius, we write the numberdensity of protons as a function of energy, $n_p(r, \gamma)$, as the product of a normalized velocity distribution, which depends on the temperature at each radius, and the total numberdensity of protons (see eg. Mahadevan et al. 1997),

$$n_p(r, \gamma) = n_p(r) n_\gamma[\gamma, \theta_p(r)], \quad (16)$$

with

$$\int_1^\infty n_\gamma[\gamma, \theta_p(r)] d\gamma = 1, \quad \int_1^\infty (\gamma - 1) n_\gamma[\gamma, \theta_p(r)] d\gamma = \frac{3}{2} \theta_p(r). \quad (17)$$

The total numberdensity of protons, $n_p(r)$, is determined from equation (13), and for the present results we consider a normalized velocity distribution, $n_\gamma[\gamma, \theta_p(r)]$ which is either a relativistic Maxwell–Boltzmann or power–law distribution. With this functional form of $n_p(r, \gamma)$, equations (2) and (4) can be evaluated to give the total production of e^\pm , and therefore the total synchrotron emission.

Determining the synchrotron spectrum from the e^\pm in an ADAF, requires three additional pieces of physics to those presented in §2. First, the emergent spectrum at radii close to the black hole must be corrected for gravitational redshift effects. This is included in the calculations that follow, and has the effect that $L_\nu^s(\nu)$ observed at large radii is now $L_\nu^s[\nu(1 - 1/r^{1/2})]$. This shifts L_ν^s redward by the gravitational redshift factor. The inclusion of gravitational redshift will change the entire optically thin synchrotron spectrum determined in §2.3. However, this will only affect the spectrum dramatically within a few Schwarzschild radii.

Second, in addition to calculating the optically thin synchrotron spectrum at each radius in the flow (§2.3), absorption processes also need to be included. This will change the resulting synchrotron spectrum at frequencies where the plasma is optically thick. In particular, since the thermal electrons in an ADAF radiate highly self–absorbed synchrotron emission (Narayan & Yi 1995b; see also Mahadevan 1997), these electrons will absorb any radiation that is above the local black body value. Therefore, to account for this absorption process we replace any “excess” synchrotron emission from the e^\pm with the local black body spectrum at each radius. In a highly self–absorbed plasma, this is a good approximation to the exact radiative transfer calculations.

In addition to the absorption process described above, self–absorption by the created e^\pm is also included. However, in the calculations that follow, we find that absorption from the thermal electrons is always more important. Since the amount of absorption depends on the physical size of the emitting region, the calculations for the rest of this

section are for a black hole mass $m = 10^6$, accreting at a rate $\dot{m} = 10^{-4}$. §4 explores the results for different black hole masses and accretion rates.

Finally, the calculations and spectra discussed in §2 assumes that a steady state distribution has been established. The only timescale of interest there was the synchrotron cooling time. However, in an ADAF, the accretion time, t_{ac} , is another important timescale in the problem. If the synchrotron cooling time is longer than the accretion time, a steady state distribution will not be able to form, and while the e^\pm will still radiate synchrotron emission, the spectral results of §2 are no longer valid. Setting the synchrotron cooling time $t_s = \gamma/\dot{\gamma}_s \simeq 7.4 \times 10^8/\gamma B^2$, equal to the accretion time $t_{ac} \simeq 1.8 \times 10^{-5} \alpha^{-1} m r^{3/2}$ (Mahadevan & Quataert 1998), gives

$$\dot{m} \gtrsim 4 \times 10^{-4} \left(\frac{\alpha}{0.3} \right)^2 \left(\frac{\gamma}{200} \right)^{-1} \left(\frac{r}{10^4} \right) \left(\frac{1 - \beta_{\text{adv}}}{0.5} \right)^{-1}, \quad (18)$$

where we have used the self-similar scaling of the magnetic field with radius (Narayan & Yi 1995b; see also Mahadevan 1997), and have set $\gamma \sim 200$, the Lorentz factor of the e^\pm responsible for most of the radiation (cf. Fig. 1e). For systems where $\dot{m} \gtrsim 10^{-4}$, the timescale for the e^\pm to cool via synchrotron radiation is less than the accretion time, and a steady state distribution will be established. The results of §2 are therefore valid. For lower accretion rates, the spectrum will be modified, but we do not consider this regime since the luminosities from these systems will be too low to be of observational consequence. All published models of ADAFs in the literature have $\dot{m} > 10^{-4}$.

3.2.1. Thermal Distribution

Using equation (13) the synchrotron emissivity per unit scaled volume in an ADAF is given by

$$L_\nu = \frac{dE}{dt d\tilde{V} d\nu} = 2.57 \times 10^{16} m \dot{m}^2 \tilde{n}_p^2(r) L_\nu^s \quad \text{erg s}^{-1} \text{ Hz}^{-1}, \quad (19)$$

where L_ν^s is the synchrotron emissivity for $n_p = 1 \text{ cm}^{-3}$ (cf. eq. [11]), and $dV = (2.95 \times 10^5)^3 m^3 d\tilde{V}$. Here, $d\tilde{V} = 4\pi r^2 dr$, is the scaled volume in Schwarzschild units. The dependence of L_ν on the energy distribution of the protons is taken into account by the form of $R(E_{e^\pm})$ that is used to evaluate L_ν^s (cf. Figure 1a). As expected, equation (19) shows that the luminosity of the optically thin part of the spectrum increases as $m \dot{m}^2$ similar to the γ -ray spectrum (Mahadevan et al. 1997). However, this scaling is no longer valid for frequencies where the spectrum is self-absorbed.

All the emission is produced in the inner most regions of the flow ($r \lesssim 5$) where the proton temperatures are high enough to produce pions. At larger radii, the temperatures drop rapidly, and almost none of the protons have energies above the threshold for pion production (cf. §2). Since the e^\pm synchrotron emission originates from a few Schwarzschild radii, all the self-absorption is from the thermal electrons at $r \lesssim 5$.

Figure 2a shows the results for two values of the viscosity parameter α (0.1 and 0.3) and two values of β_{adv} (0.5 and 0.9). At relatively high frequencies, the spectra are optically thin and show the characteristic rise ($\nu L_\nu \propto \nu^{+0.5}$) and exponential turnover expected from a thermal proton distribution (§2, Fig. 1c). At lower frequencies, however, the emission is highly self-absorbed by the ambient thermal electrons. The resultant self-absorbed spectrum is Rayleigh–Jeans and has a spectral dependence $\nu L_\nu \propto \nu^3$. Although the distinct spectral change offers an interesting testable prediction, the luminosity from this process is negligible compared with the synchrotron luminosity from the thermal electrons at these frequencies. The thermal e^\pm spectrum is therefore undetectable (see §4).

For a given α , increasing β_{adv} leads to an increase in gas pressure, which therefore increases the proton temperature (cf. eq.[15]). Changing β_{adv} from 0.5 to 0.9, causes the temperature to increase by a factor ~ 2 , and since the e^\pm flux is extremely sensitive to temperature (cf. §2), the synchrotron flux increases by nearly 2 orders of magnitude. For a fixed β_{adv} , changing α also affects the synchrotron luminosity. Since π^\pm production scales as $n_p^2 \propto \alpha^{-2}$ (Narayan & Yi 1995b), we might expect that decreasing α increases the total luminosity. In the case of high β_{adv} this is the case, but in the more detailed global solutions in the Kerr metric, the slight change in temperature with α in the innermost regions of the flow, for low β_{adv} , compensates for the increase in numberdensity, and the net result is a decrease in the total flux.

3.2.2. Power-Law Distribution

For a power-law distribution of protons, the total number of protons is still given by equation (13), but the distribution $n_\gamma[\gamma, \theta_p(r)]$ is no longer Maxwellian. Following Mahadevan et al. (1997) we write the energy distribution of protons as

$$n[\gamma, \theta_p(r)] d\gamma = \left\{ [1 - \zeta(r)] \delta(\gamma - 1) + (s - 1) \zeta(r) \gamma^{-s} \right\} d\gamma, \quad (20)$$

where a fraction $1 - \zeta(r)$ of the protons have $\gamma \sim 1$, and a fraction $\zeta(r)$ are in a power-law tail with index s . The fraction $\zeta(r)$ is fixed by the energy requirement (cf. eq. [17]):

$$\zeta(r) = \frac{3}{2} (s - 2) \theta_p(r). \quad (21)$$

Using equation (20) in equation (2) gives the total charged pion spectrum. In an ADAF, $\zeta \ll 1$, and Mahadevan et al. (1997) have shown that most of the contribution to the pion spectrum comes from protons in the power-law tail colliding with protons at rest. Equation (20) can therefore be simplified to

$$n[\gamma, \theta_p(r)] d\gamma \simeq (s - 1) \zeta(r) \gamma^{-s} d\gamma,$$

and the e^\pm synchrotron emissivity per unit scaled volume takes the form

$$L_\nu = \frac{dE}{dt d\tilde{V} d\nu} = 2.57 \times 10^{16} m \dot{m}^2 \tilde{n}_p^2(r) \zeta(r) [1 - \zeta(r)] L_\nu^s, \quad (22)$$

where L_ν^s represents the synchrotron emissivity using a proton distribution $n(\gamma) = (s - 1)\gamma^{-s}$ (cf. eq.[11] and Fig. 1f).

Figure 2b shows the resulting spectrum for a proton energy distribution with power-law index $s = 2.75$ for different values of $\alpha = (0.1, 0.3)$ and $\beta_{\text{adv}} = (0.5, 0.9)$. Similar to the thermal case, the optically thin part of the spectrum scales as $m \dot{m}^2$ (cf. eq.[22]), but at lower frequencies this scaling is no longer valid since the spectrum is self-absorbed. For a fixed α increasing β_{adv} decreases the magnetic field which shifts the spectrum to lower frequencies (§2.3, Fig. 1f). For fixed β_{adv} decreasing α increases the numberdensity ($n_p \propto \alpha^{-1}$) which increases the optically thin flux.

Unlike the thermal case, the emission comes from nearly all radii in the ADAF. In particular, since the protons are assumed to be accelerated into a power-law at all radii, most of the high frequency emission originates from $r \lesssim 30$ while the low frequency emission comes from $r \lesssim 10^4$. To understand this effect, recall that an e^\pm with Lorentz factor γ radiates most of its energy at frequencies $\nu \propto \gamma^2 B$. Since γ is fixed at all radii by the microphysics of particle decays (§2 and Fig. 1d), the frequency at which most of the synchrotron radiation emerges depends only on the magnetic field. As the magnetic field decreases with increasing radius, lower frequency emission occurs farther away from the black hole.

At relatively high frequencies, the spectra are optically thin and show the characteristic rise ($\nu L_\nu \propto \nu^{+0.5}$), turnover, and power-law tail ($\nu L_\nu \propto \nu^{-s/2}$) expected from a power-law proton distribution (§2, Fig. 1f). At lower frequencies, however, the emission is highly self-absorbed by the ambient thermal electrons, and predicted spectrum is determined by self-absorption at all radii (§3.2). We show below (§§4 and 5) that the expected spectral shape provides an interesting prediction for the ADAF paradigm, and in the case of our Galactic Centre, Mahadevan (1998) has shown that these predictions do indeed agree quite well with the observations.

4. Results: Application to Solar and Supermassive Black Holes

This section combines the spectra produced by both the protons and electrons in an ADAF. The bulk of the electrons cool via thermal synchrotron, bremsstrahlung and inverse Comptonization (Narayan & Yi 1995b; see also Mahadevan 1997), while the protons cool via the production of neutral and charged pions. In the results that follow, the γ -ray spectrum, produced by the decay of neutral pions, has been updated from Mahadevan et al. (1997) to include general relativistic effects, gravitational redshift, and the non-spherical geometry of the flow (§3).

4.1. Thermal Distribution

For a thermal distribution of protons, Figure 3a shows the total spectrum from ADAFs around various black hole systems corresponding to $m = (10, 10^6, 10^9)$ and $\dot{m} = (10^{-2}, 10^{-4})$. The solid, dashed and dotted lines correspond respectively to the total emission from the ADAF, the emission from the bulk of the thermal electrons, and the emission from the e^\pm . As expected, the low proton temperatures in an ADAF do not allow for a significant amount of e^\pm synchrotron emission, and the luminosities are too low to be of observational interest.

4.2. Power–Law Distribution

For a power–law distribution of protons, Figure 3b shows the total spectrum from ADAFs around the same black hole systems corresponding to $m = (10, 10^6, 10^9)$ and $\dot{m} = (10^{-2}, 10^{-4})$. The solid, dashed and dotted lines correspond respectively to the total emission from the ADAF, the emission from the bulk of the thermal electrons, and the emission from the e^\pm , for the three different values of the proton energy index s . The heavy solid line corresponds to the total ADAF spectrum for $s = 2.75$. Unlike the thermal case, the power–law e^\pm do produce significant amounts of detectable emission.

For all black hole masses, Figure 3b shows that bremsstrahlung emission from the thermal electrons has a cutoff at $h\nu \sim kT_e$, which corresponds to $\nu \sim 10^{20}$ Hz, and inverse Compton scattering of the electrons also turns over at these frequencies due to the decrease in the Klein–Nishina cross–section. The emission for $\nu \gtrsim 10^{20}$ Hz is therefore only due to proton cooling. All spectra show that the e^\pm naturally provide a hard power–law tail which extends up to ~ 100 MeV. Beyond these energies, the decay of neutral pions into γ –rays dominate the spectrum, and produce a distinct rise in the spectrum which turns over at a few GeV and extends as a power–law to very high energies. An interesting consequence is that although the spectral index of the MeV and GeV spectrum are different, they are not independent of each other. For a parent proton distribution with energy index s , the MeV and GeV spectrum have spectral dependencies $\nu L_\nu \propto \nu^{-s/2}$ and $\nu^{-(s-2)}$ respectively (Mahadevan et al. 1997).

For frequencies $\nu \lesssim 10^{20}$ Hz, the dominance of the proton cooling spectrum, compared with the emission from the thermal electrons, depends sensitively on the accretion rate \dot{m} , and to a lesser degree on the mass m of the black hole. For low mass black holes (eg. Cyg X–1, A0620) the proton cooling spectrum is almost always unobservable for all accretion rates. For higher mass black holes, however, the proton cooling emission is observable for $\nu \lesssim 10^{11}$ Hz and between $10^{14} – 10^{17}$ Hz, and depends crucially on \dot{m} .

For supermassive black holes, Figure 3b shows that between frequencies $10^{14} – 10^{17}$ Hz, the turn over in the e^\pm synchrotron spectrum, is observable only for low accretion rate

systems. Increasing the accretion rate, increases the amount of thermal inverse Compton scattering ($\propto \dot{m}^3$; Narayan & Yi 1995b; Mahadevan 1997), which increases faster than the amount of e^\pm synchrotron radiation ($\propto \dot{m}^2$). The luminosity from thermal inverse Compton scattering will therefore dominate the spectrum at these frequencies. The e^\pm spectrum is therefore unobservable for high accretion rate AGN such as NGC 4258 ($\dot{m} \sim 0.01$; Lasota et al. 1996), while the spectrum dominates the infrared to soft X-ray band for low accretion rate systems like our Galactic centre ($\dot{m} \sim 10^{-4}$, Narayan et al. 1998b; Mahadevan 1998).

For frequencies $\nu \lesssim 10^{11}$ Hz, the radio spectrum from ADAFs around supermassive black holes is substantially modified by the radiating e^\pm . Figure 3b shows that the additional synchrotron emission has two effects: (1) it increases the radio flux by as much as an order of magnitude at certain frequencies, and (2) changes the shape of the spectrum by producing an observable spectral break. As discussed in §5, Mahadevan (1998) has shown that the observed spectral break from radio observations of the Galactic centre (Sgr A*) can be explained quite well by e^\pm synchrotron radiation.

It is interesting that the synchrotron radiation from the e^\pm actually produce more emission at low radio frequencies than the thermal electrons. Since the thermal electrons radiate highly self-absorbed synchrotron emission, the emission at each frequency in the radio, ν_f , corresponds to black body emission at a definite radius, r_f (Mahadevan 1997). Any “excess” emission that is greater than the local black body value will be highly self-absorbed. In this case, how does the inclusion of synchrotron radiation from the e^\pm increase the radio emission? The apparent paradox is resolved by noting that the enhanced emission at ν_f results from the high energy e^\pm radiating synchrotron emission at larger radii, $r > r_f$. While any excess radiation emitted at $r < r_f$ is completely self-absorbed by the thermal electrons at r_f , the e^\pm at radii $r > r_f$ radiate most of their energy at $\nu \sim \gamma^2 \nu_B \sim \nu_f$, which is now optically thin to the local black body, and free to escape from the plasma. The excess radio emission therefore comes from high energy e^\pm radiating at larger radii.

5. Discussion and Conclusions

ADAFs are the only hot accretion flow models that attempt to self-consistently incorporate the viscous hydrodynamics, thermal structure, and radiative processes in the inflowing gas. The models have been worked out in considerable detail, and the success of ADAFs therefore lies in their ability to make robust observational predictions. The numerous applications of ADAFs to solar and supermassive black holes (eg. Di Matteo et al. 1998; Esin et al. 1997, 1998; Fabian & Rees 1995; Reynolds et al. 1996; Narayan et al. 1995; see Narayan et al. 1998a for a review) have not only led us to a better understanding of these systems, but have also reinforced our belief that ADAFs are a substantial step in the right direction, towards a possibly more detailed solution of low

luminosity accreting systems.

In order for the ADAF solutions to exist two basic assumptions in plasma physics must be satisfied: (1) the existence of a hot two temperature plasma, and (2) the viscous energy generated primarily heats the protons. If either of these assumptions fail, then the ADAF solution, and the resulting spectra that they produce, cease to exist. To understand this, consider first the existence of a two temperature plasma. In an ADAF, all the viscous energy is stored in the protons of the gas and only a small fraction of this energy is transferred to the electrons to be radiated away. This fraction is determined by Coulomb collisions and the large temperature difference of the protons and electrons. If some other mechanism (eg. a plasma instability) is more efficient in coupling the protons and electrons to equilibrate their temperatures, then all the stored energy in the protons, would be transferred to the electrons to be radiated away. No energy will be advected with the accreting gas, the accretion flow becomes very luminous, and the ADAF solution does not exist.

Second, the protons become hot and advect the viscous energy because viscosity is assumed to primarily heat the protons. If the viscously dissipated energy went into heating the electrons instead, then this energy would be immediately radiated away, resulting in a luminous system. Again, no energy would be advected by the gas, and the ADAF solution does not exist. The validity of these assumptions are therefore crucial for the existence of ADAFs.

This paper has focussed on providing additional observational tests for these two assumptions, by presenting detailed spectra from both the protons and electrons. We have concentrated on the cooling of protons via the production of charged pions, which subsequently decay into positrons and electrons. These particles interact with the local magnetic fields to produce synchrotron radiation. Until recently, observational signatures of hot protons was relegated to very high energies, where neutral pions decay to produce gamma-rays (\sim few GeV). The present results not only probe the two temperature paradigm further, but also allow us to predict the existence of hot protons in a more observationally tractable regime of the electromagnetic spectrum.

It is important to understand the connection between the spectra from the protons and electrons in ADAFs. Once the spectrum from the thermal electrons is determined, all the parameters in the ADAF are fixed. Properties of the gas such as the numberdensity, temperatures, and magnetic field strengths, cannot be changed, and the resultant spectra from proton cooling depends only on the physical processes in the plasma. In particular, the energies of the created e^\pm , their steady state numberdensity distributions, and shape of the resulting synchrotron spectra (cf. Fig. 1), depend only on the microphysics of particle collisions, decays, and radiative processes. It is this strong interplay between the proton and electron spectra that allows testable predictions of the basic assumptions of ADAFs, and also allows a probe into the proton energy distribution in these flows.

Since it is not understood whether viscous heating produces a thermal or power-law distribution of proton energies, we have calculated the e^\pm spectrum due to both distributions; the true distribution will be some combination of the two, and can be determined by taking the weighted sum of the thermal and power-law spectra. Recently, there have been a number of theoretical investigations which consider particle heating in ADAFs (Bisnovatyi-Kogan & Lovelace 1997; Blackman 1998; Quataert 1998; Gruzinov 1998; Quataert & Gruzinov 1998; see Narayan et al. 1998a for a review), some of which also argue for and against both proton distributions. Here, we have attempted to answer this question observationally by providing accurate spectra from these distributions.

If the proton distribution is thermal, the resulting e^\pm synchrotron spectrum peaks between frequencies $10^{12} - 10^{17}$ Hz, and produces very low luminosities. In addition, the radiation by the thermal electrons dominates the emission from the radio to hard X-rays, which results in an e^\pm spectrum that is completely unobservable (Fig. 3a). In this case, the only observable signature of hot protons would be in the gamma-rays, but the predicted fluxes are much too low to be detected even by the next generation gamma-ray telescope, GLAST.

However, if the protons have a power-law distribution of energies, the e^\pm synchrotron spectrum can be observed. For supermassive black holes, the emission appears in the radio, and, depending on the accretion rate, also between infrared and soft X-ray energies. In particular, the best systems to look for such radiation would be in supermassive black holes with low accretion rates. Fortunately, the supermassive black hole at our Galactic centre (Sgr A*) offers such an opportunity. It is the closest low luminosity AGN that we know, and has been observed quite extensively.

Recently, Narayan et al. (1998b) have used an ADAF model to explain the spectrum and low luminosity from Sgr A*. For the canonical values of $\alpha = 0.3$ and $\beta = 0.5$, and the dynamically measured mass $M = 2.5 \times 10^6 M_\odot$ (Haller et al. 1996; Eckart & Genzel 1997), they vary just one free parameter, \dot{m} , to fit the X-ray flux, and show that the resulting spectrum from the thermal electrons explains the low luminosity and observed broad band spectrum quite well. The model, however, has difficulties in explaining the non-uniform radio spectrum. It is important to realize that once the thermal electron spectrum is fixed, all the parameters in an ADAF are determined, and there are no more free parameters available. The non-uniform radio spectrum has therefore always been unexplained by the ADAF model.

This discrepancy has recently been solved by considering e^\pm synchrotron emission from the ADAF around Sgr A* (Mahadevan 1998). Without changing any parameters, and just including another physical process – e^\pm synchrotron emission from a power-law proton distribution, Mahadevan (1998) shows that the ADAF model naturally reproduces the observed radio spectral break at ~ 86 GHz, and accounts for the low frequency luminosities. This is shown by the solid line in Figure 4, which provides quite compelling evidence that a two temperature plasma probably does exist in an ADAF around Sgr

A*. More importantly, the results provide, for the first time, observational support for the basic assumptions in an ADAF (Mahadevan 1998).

While one of the ADAF assumptions requires almost all of the viscous energy to be transferred to the protons, it does not indicate whether this energy should heat the protons into a power–law or thermal distribution. This depends on the details of viscous heating, and it is interesting that the recent results from Sgr A* allows an observational answer to this question. If we characterize the amount of viscous energy that goes into a power–law by Δ , then the case when no energy goes into the power–law distribution is $\Delta = 0$, which is shown in Figure 3a; $\Delta = 1$ corresponds to Figure 3b. The question arises as to what the most likely values of Δ can be, ie. how much of the viscous heating is transferred to a power–law distribution and how much to a thermal one. To assess this, we use the results of Mahadevan (1998) as our baseline model. $\Delta = 1$ corresponds to the solid line in Figure 4, while $\Delta = 0$ corresponds to the long dashed line (Narayan et al. 1998b). The dotted, short dashed, and dot dashed lines correspond to spectra for $\Delta = 0.5, 0.25$, and 0.1 respectively.

Figure 4 shows that the results are not very sensitive to Δ ; this factor will only appear linearly in equation (21). While the luminosity of the optically thin part of the power–law spectrum decreases linearly with Δ , the self–absorbed radio part is less sensitive. For $\Delta \gtrsim 0.3$, the agreement with the radio spectrum does not change significantly. This implies that the observations are consistent with approximately a third or more of the viscous energy going into a power–law distribution of protons, and the rest into a thermal or quasi–thermal one. The results therefore provide clues to the physics of viscous heating in these flows, and could be used as tools to aid future theoretical work in resolving some of the complex questions in plasma physics.

The results of Mahadevan (1998) encourages us to adopt the view that the protons in an ADAF, might in fact have a power–law distribution in energies. This gives rise to numerous testable predictions in the fluxes in various wavebands as well as the spectral shapes. First, all spectra from two body emission processes, in the optically thin limit, must have constant ratios in their fluxes. This is a result of all two body processes varying as the square of the density. The three processes in an ADAF, which depend on the square of the density, are bremsstrahlung emission and the creation of neutral and charged pions. From Figure 3b it is clear that these three processes always have the same relative amplitudes in the optically thin regime ($\nu \gtrsim 10^{10}$ Hz). In particular the ratio of the gamma–ray to bremsstrahlung to e^\pm synchrotron fluxes are all the same, and are determined essentially by the ratios of their respective cross–sections and rates. While the cross–section for charged pion creation is greater than that for neutral pions, the synchrotron spectrum from the e^\pm has a lower peak flux than the γ –rays. This is due to the synchrotron radiation being emitted over a much broader frequency range.

For low accretion rate systems, these emission processes dominate the radiation for frequencies $\nu \gtrsim 10^{12}$ Hz, which provides strong testable correlations among the fluxes in

the optical, X-rays, hard X-rays, and γ -ray bands. Further, changes in the accretion rate, leads to changes in the the densities, which would result in simultaneous variations in the fluxes at these different frequencies. Observations of such variability would provide very interesting tests of the ADAF paradigm. It is apparent from Figure 3b that the best laboratories to verify these predictions would be in low luminosity AGN.

In addition to the predicted correlation in fluxes, there are also correlations in the expected spectral shapes and slopes. As discussed in §4, the ubiquitous presence of a hard power-law at \sim MeV and \sim GeV energies provides two independent checks on the distribution of protons. In an ADAF the detection of one requires the presence of the other. The power-law spectra presented here do not show any high energy cutoff. This is a direct consequence of postulating a power-law proton distribution which extends to very high energies. However, if we arbitrarily postulate a maximum proton energy (for example the energy at which the proton gyroradius equals the size of the ADAF) then the resulting spectra would also show a corresponding cutoff.

The increased radio flux, from supermassive black holes, due to e^\pm radiation, facilitates easier comparisons with observations, and can be used to constrain the sizes of ADAFs in AGN. Recently, Herrnstein et al. (1998) have compared observational upper limits to the 22 GHz emission from NGC 4258 with an ADAF model, and conclude that an ADAF cannot have radii larger than ~ 100 Schwarzschild. We might expect that the current results would produce more emission in the radio, and the size of the ADAF would therefore be further reduced. However, this is not the case since in order to produce more emission at 22 GHz, requires synchrotron radiation from e^\pm at radii $r \gtrsim 100$. In fact the current results allows for a more definite upper limit to the size of the ADAF deduced by Herrnstein et al. (1998), since a larger outer radius implies more emission at 22 GHz from the e^\pm . This technique can also be used to constrain, or establish, the existence of ADAFs at the cores of nearby low luminosity ellipticals.

Finally, we discuss two physical processes that have been neglected: (1) inverse Compton scattering of soft photons by the created e^\pm , and (2) the observational importance of an annihilation line. First, the significance of inverse Compton scattering, by the created e^\pm , is determined by comparing the ratio of the total inverse Compton power to synchrotron power, $P_{\text{Com}}/P_{\text{syn}} = U_{\text{ph}}/U_B$, where U_{ph} , U_B are the photon and magnetic field energy densities respectively. For an ADAF, $U_{\text{ph}}/U_B \sim L_{\text{emitted}}/L_{\text{advected}} \ll 1$, where L_{emitted} , L_{advected} are the emitted and advected luminosities, respectively, and inverse Compton scattering of the e^\pm is therefore not energetically important.

Second, assessing the observational importance of an annihilation line requires a knowledge of the total energy in the line, as well as the line width. Since the annihilation cross-section is greatest for Lorentz factors $\gamma \sim 1$, and most of the synchrotron emission occurs from electrons with $\gamma \sim 200$, the power in the annihilation line will be $\sim P_{\text{syn}}/200$. In the case of Sgr A* this corresponds to $\sim 10^{33}$ erg s $^{-1}$. If the width of the line is narrow, then the line will be observable. However, the e^\pm that annihilate have thermalized

with the ambient electrons at temperatures $\sim 10^{9.5}$ K. At such high temperatures, the annihilation line is sufficiently broadened ($\Delta E/E = \sqrt{2kT_e/m_e c^2} \sim 1$ MeV), which results in a spectral line that is unobservable.

Acknowledgments: I thank Ramesh Narayan and Andy Fabian for useful discussions.

REFERENCES

Abramowicz, M.A., Czerny, B., Lasota, J. P., & Szuszkiewicz, E., 1988, *ApJ*, 332, 646

Abramowicz, M.A., Chen, X., Kato, S., Lasota, J.-P., & Regev, O. 1995, *ApJ*, 438, L37

Bhadwar, G. D., Stephens, S. A., & Golden, R. L., 1977, *Phys. Rev. D*, 15, 820

Bisnovatyi-Kogan, G.S. & Lovelace, R. V. E., 1997, *ApJ*, 486, L43

Blackman, E., 1998, *Phys. Rev. Lett.*, submitted (astro-ph/9710137) (1998)

Chen, X., Abramowicz, M. A., & Lasota, J.-P. 1997, *ApJ*, 476, 61

Chen, X., Abramowicz, M. A., Lasota, J.-P., Narayan, R., & Yi, I. 1995, *ApJ*, 443, L61

Dermer, C. D., 1986a, *ApJ*, 307, 47

Dermer, C. D., 1986b, *A&A*, 157, 223

Di Matteo, T., Fabian, A. C., Rees, M. J., Carilli, C. L., & Ivison, R. J., 1998, *MNRAS*, submitted (astro-ph/9807245)

Eckart, A., & Genzel, R. 1997, *MNRAS*, 284, 576

Esin, A. A., Narayan, R., Cui, W., Grove, J. E., & Zhang, S. N., 1998, *ApJ*, in press (astro-ph/9711167)

Esin, A. A., McClintock, J. E., & Narayan, R. 1997, *ApJ*, 489, 865 (Erratum: 1998, *ApJ*, 500, 523)

Fabian, A. C., & Rees, M. J., 1995, *MNRAS*, 277, L55

Gammie, C., & Popham, R. 1998, *ApJ*, 498, 313

Ginzburg, V. L., & Syrovatskii, S. I., 1964, *The Origin of Cosmic Rays*, (New York: Macmillan)

Gruzinov, A., 1998, *ApJ*, 501, 787

Haller, J. et al., 1996, *ApJ*, 456, 194 (Erratum: 1996, *ApJ*, 468, 955)

Herrnstein, J. R. et al., 1998, *ApJ*, 497, L69

Ichimaru, S., 1977, *ApJ*, 214, 840

Landau, L. D., & Lifshitz, E. M., 1975, *The Classical Theory of Fields*, 4th Ed., (Pergamon: Oxford)

Lasota, J. P., Abramowicz, M. A., Chen, X., Krolik, J., Narayan, R., & Yi, I., 1996, *ApJ*, 462, 142

Lindenbaum, S. J., Sternheimer, R. M., 1957, *Phys. Rev.*, 105, 1874

Mahadevan, R. 1998, *Nature*, 394, 651

Mahadevan, R. 1997, *ApJ*, 477, 585

Mahadevan, R., Narayan, R., & Krolik, J. 1997, *ApJ*, 486, 268

Mahadevan, R., & Quataert, 1997, *ApJ*, 490, 605

Narayan, R. 1996, in *Physics of Accretion Disks*, ed. S. Kato, S. Inagaki, S. Mineshige & J. Fukue (Gordon & Breach), 15

Narayan, R., Barret, D., & McClintock, J. E. 1997, *ApJ*, 482, 448

Narayan, R., Kato, S., & Honma, F. 1997, *ApJ*, 476, 49

Narayan, R., Mahadevan, R., & Quataert, E., 1998a, in *The Theory of Black Hole Accretion Discs*, eds. M. A. Abramowicz, G. Bjornsson, & J. E. Pringle, in press (Cambridge Univ. Press) (astro-ph/9803141)

Narayan, R., Mahadevan, R., Grindlay, J. E., Popham, R. G., & Gammie, C., 1998b, *ApJ*, 492, 554

Narayan, R., McClintock, J. E., & Yi, I. 1996, *ApJ*, 457, 821

Narayan, R., & Yi, I. 1994, *ApJ*, 428, L13

Narayan, R., & Yi, I. 1995a, *ApJ*, 444, 231

Narayan, R., & Yi, I. 1995b, *ApJ*, 452, 710

Narayan, R., Yi, I., & Mahadevan, R. 1995, *Nature*, 374, 623

Popham, R., & Gammie, C. 1998, *ApJ*, 504, 419

Quataert, E., 1998, *ApJ*, 500, 978

Quataert, E. & Gruzinov, A., 1998, *ApJ*, submitted (astro-ph/9803112)

Ramaty, R., & Lingenfelter, R. E., 1966a, *J. Geophys. Res.*, 71, 3687

Ramaty, R., & Lingenfelter, R. E., 1966b, *Phys. Rev. Lett.*, 17, 1230

Ramaty, R., & Lingenfelter, R. E., 1968a, *Phys. Rev. Lett.*, 20, 120

Rees, M. J., Begelman, M. C., Blandford, R. D., & Phinney, E. S. 1982, *Nature*, 295, 17

Reynolds, C. S., Di Matteo, T., Fabian, A. C., Hwang, U., & Canizares, C. R., 1996, *MNRAS*, 283, L111

Rybicki, G., & Lightman, A., 1979, *Radiative Processes in Astrophysics* (New York: Wiley)

Shakura, N. I., & Sunyaev, R. A., 1973, *A&A*, 24, 337

Shapiro, S.L., Lightman, A.P., & Eardley, D.M. 1976, *ApJ*, 204, 187

Stephens, S. A., & Badhwar, G. D., 1981, *Astrophysics and Space Sciences*, 76, 213

Stecker, F. W., 1971, *Cosmic Gamma Rays* (Baltimore: Mono)

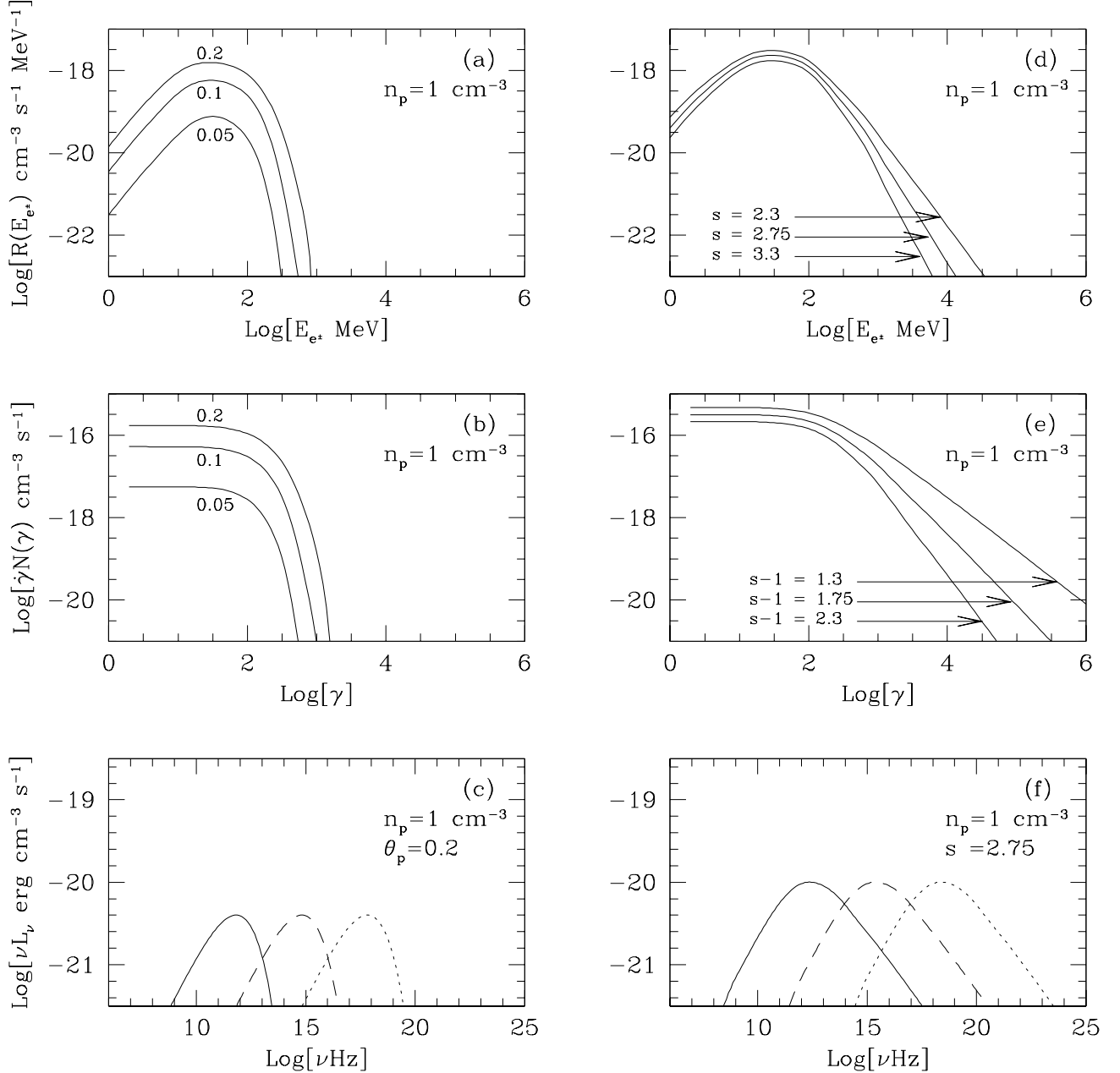


Fig. 1.— Figures showing the microphysics of e^\pm production, and the resulting synchrotron radiation. The left column is for a thermal distribution of protons where the curves are labeled by the dimensionless proton temperature, $\theta_p = kT_p/m_p c^2$. The right column is for a power-law distribution for three values of the energy index s . Figures (a) and (d) correspond the rate of creation of e^\pm for density of protons equal to unity. For a number density n , the vertical axis must be multiplied by n^2 . Figures (b) and (e) show the resulting steady state distribution $N(\gamma)$ of e^\pm . The y-axis plots $C(\gamma) = \dot{\gamma}N(\gamma)$ (cf. eq. 10). The synchrotron emission from the steady state distribution is shown in figures (c) and (f); cf. eq. 11).

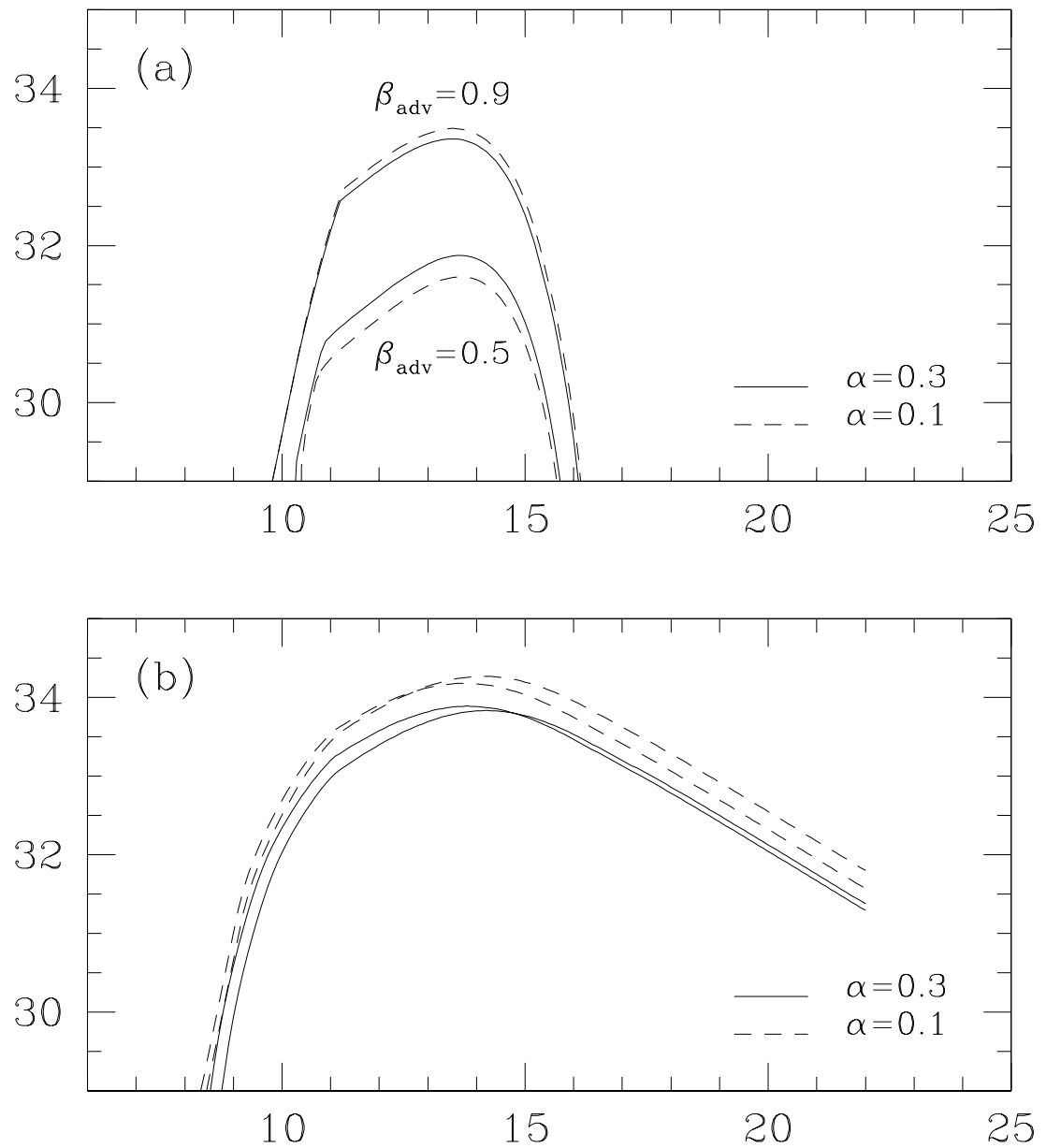


Fig. 2.— Positron and electron synchrotron spectrum from an ADAF with $m = 10^6$, $\dot{m} = 10^{-4}$, for (a) a thermal distribution of protons, and (b) a power-law distribution with energy index $s = 2.75$. In the case of a power-law distribution, the spectrum which turns over at low (high) frequencies correspond to $\beta_{\text{adv}} = 0.5$ (0.9).

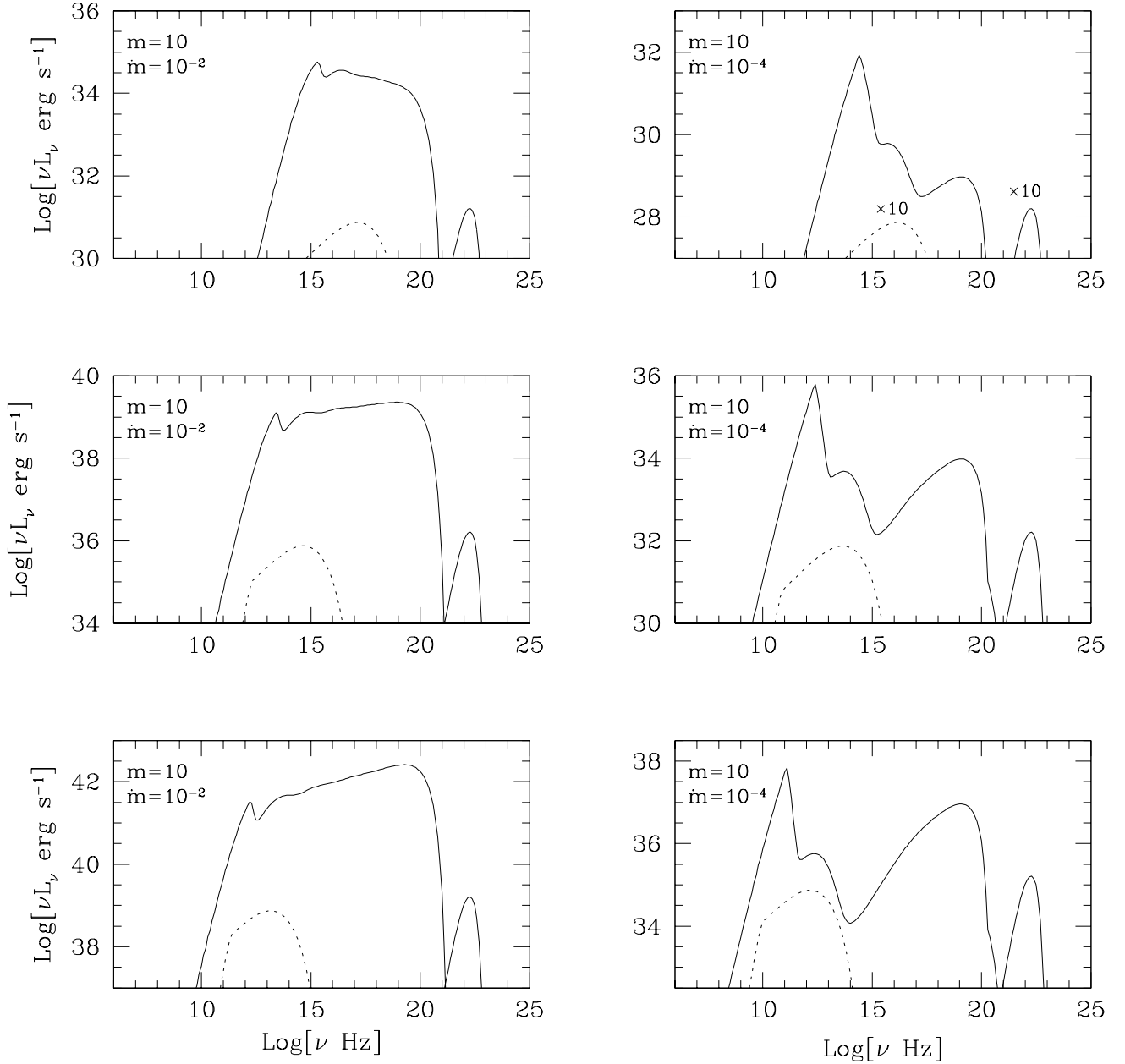


Fig. 3.— (a) Complete ADAF spectra (solid line) using a thermal distribution of protons and electrons, for different black hole masses and accretion rates. In all the calculations $\alpha = 0.3$, $\beta_{\text{adv}} = 0.5$. The e^\pm synchrotron spectrum (dotted line) is unobservable in all cases. For $(m, \dot{m}) = (10, 10^{-4})$, the γ -ray spectrum and e^\pm synchrotron spectrum have been multiplied by 10; the actual fluxes are ten times lower than shown.

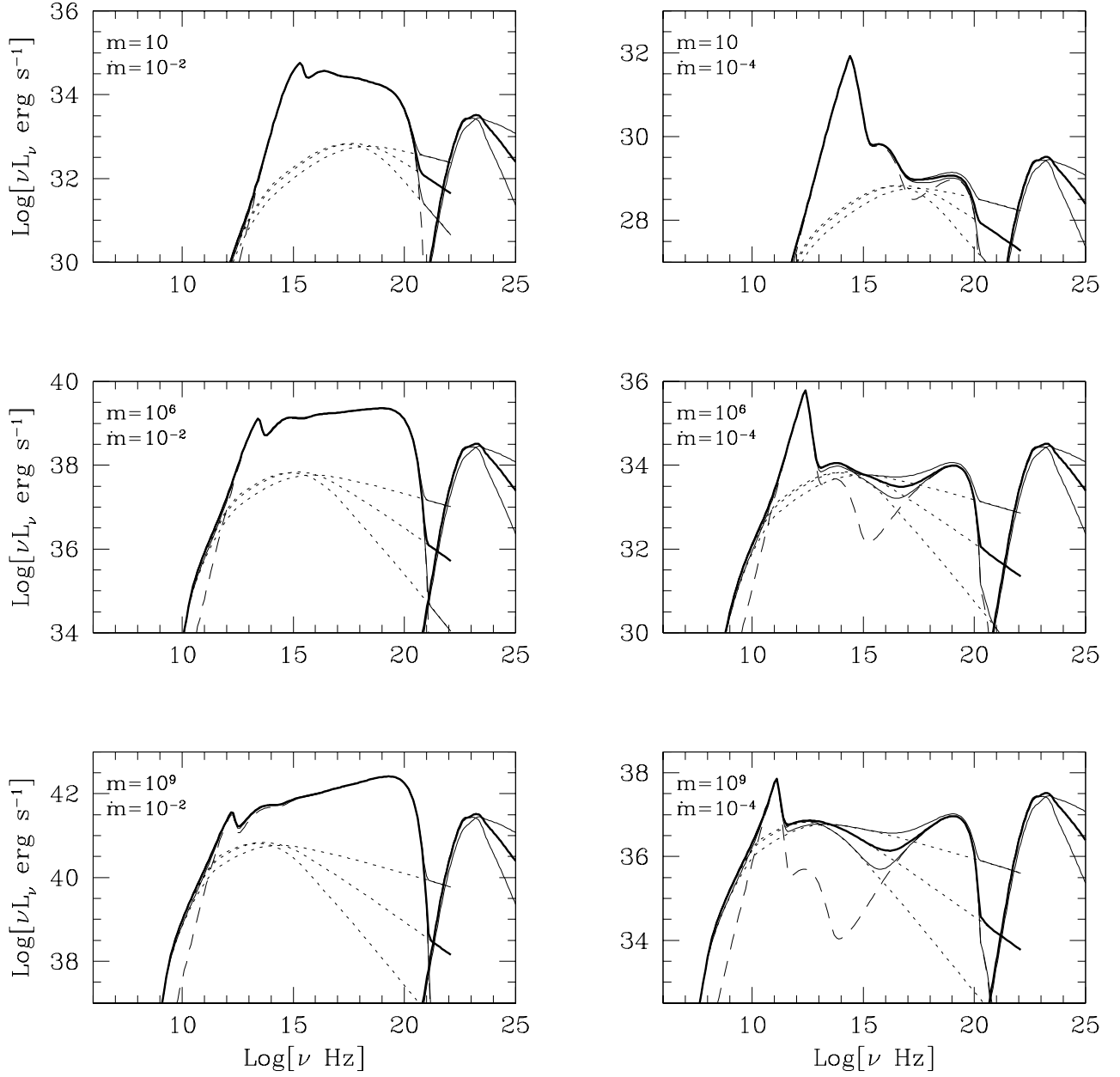


Fig. 3.— (b) Complete ADAF spectra (solid lines) using a power-law distribution of protons and thermal electrons, for the same parameters given in figure 3a. Three spectra corresponding to proton energy indices $s = 2.3, 2.75$, and 3.3 are shown. The heavy solid line represents $s = 2.75$, with the spectra below and above corresponding to $s = 3.3$ and $s = 2.3$ respectively. The dotted and dashed lines correspond to the emission from the e^\pm and the thermal electrons respectively.

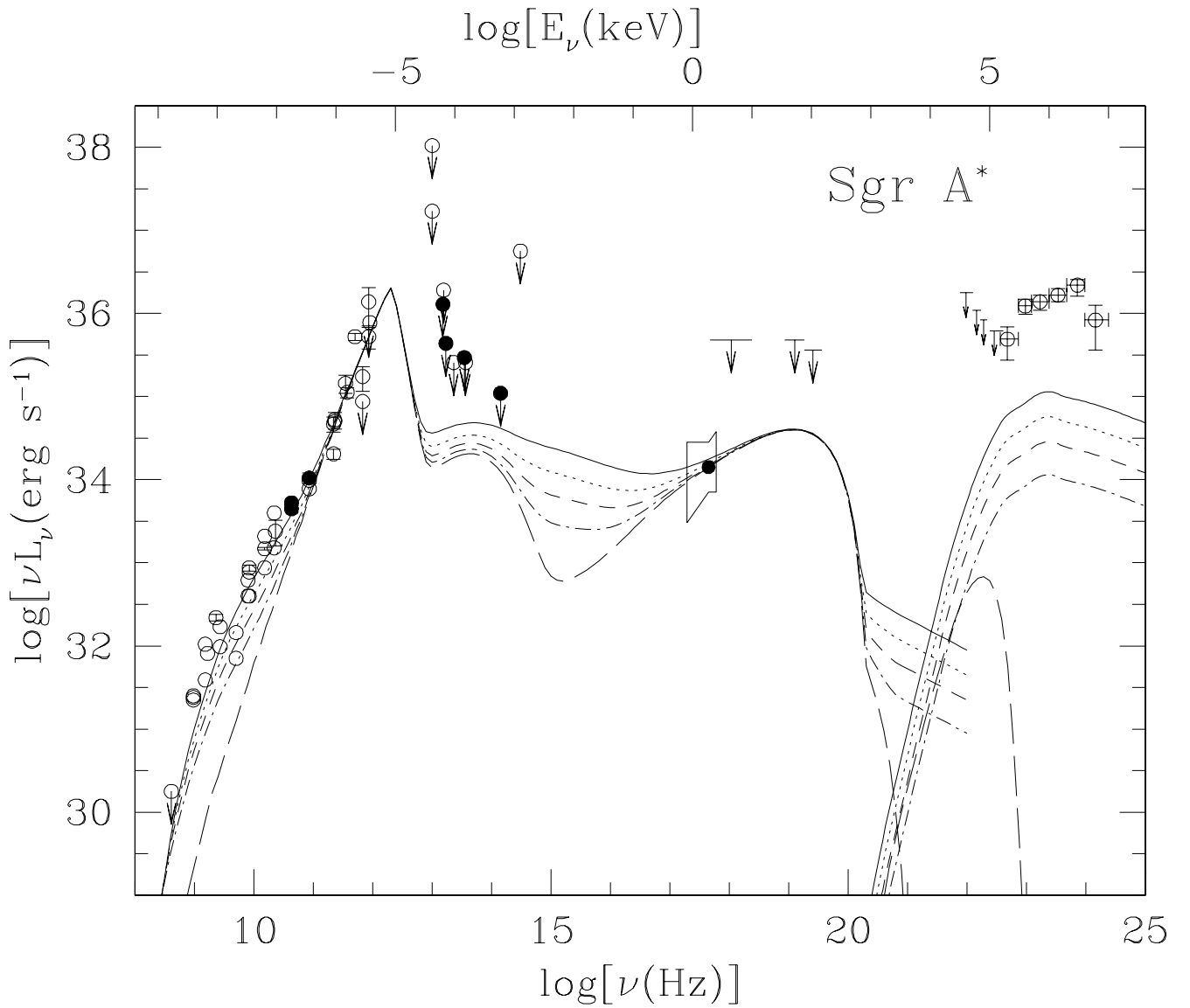


Fig. 4.— The spectrum from an ADAF around Sgr A* for different values of the parameter Δ . The data are taken from Narayan et al. (1998b). Δ is the fraction of viscous energy that heats the protons into a power-law distribution. The solid, dotted, small dashed, dot-dashed, and long dashed lines (from high to low luminosity) corresponds to $\Delta = 1.0, 0.5, 0.25, 0.1$, and, 0.0 respectively. The spectrum corresponding to $\Delta = 1$ (solid line) is taken from Mahadevan (1998).